Perry, S. V., & Cole, H. A. (1973) *Biochem. J. 131*, 425-427.
Persechini, A., & Hartshorne, D. J. (1983) *Biochemistry 22*, 470-477.
Phillips, G. N., Jr., Fillers, J. P., & Cohen, C. (1980) *Biophys. J. 32*, 485-502.
Phillips, G. N., Jr., Fillers, J. P., & Cohen, C. (1986) *J. Mol. Biol. 192*, 111-131.
Ribolow, H., & Bárány, M. (1977) *Arch. Biochem. Biophys. 179*, 718-729.
Robertson, S. P., Johnson, J. D., Holroyde, M. J., Kranias, E. G., Potter, J. D., & Solaro, R. J. (1982) *J. Biol. Chem. 257*, 260-263.
Sellers, J. R., & Adelstein, R. S. (1987) *Enzymes (3rd Ed.) 18*, 381-418.
Sellers, J. R., Chock, P. B., & Adelstein, R. S. (1983) *J. Biol. Chem. 258*, 14181-14188.
Smillie, L. B. (1979) *Trends Biochem. Sci. (Pers. Ed.) 4*, 151-155.
Stone, D., & Smillie, L. B. (1978) *J. Biol. Chem. 253*, 1137-1148.
Stull, J. T., Brostrom, C. D., & Krebs, E. G. (1972) *J. Biol. Chem. 247*, 5272-5274.

# Orientation of Actin Monomer in the F-Actin Filament: Radial Coordinate of Glutamine-41 and Effect of Myosin Subfragment 1 Binding on the Monomer Orientation†

Andrzej A. Kasprzak,* Reiji Takashi, and Manuel F. Morales
*Cardiovascular Research Institute, University of California, San Francisco, San Francisco, California 94143-0524*
*Received November 13, 1987; Revised Manuscript Received February 9, 1988*

ABSTRACT: We have employed the method of radial distance measurements in order to orient the actin monomer in the F-actin filament. This method utilizes fluorescence resonance energy transfer measurements of the distance between two equivalent chemical points located on two different monomers. The interprobe distance obtained this way is used to compute the radial coordinate of the labeled amino acid [Taylor, D. L., Reidler, J., Spudich, J. A., & Stryer, L. (1981) *J. Cell Biol. 89*, 362-367]. Theoretical analysis has indicated that if radial coordinates of four points are determined and six intramolecular distances are known, one can, within symmetry limits, position the monomer about the filament axis. The radial distance of Gln-41 that had been enzymatically modified with dansyl, rhodamine, and fluorescein derivatives of cadaverine was found to be approximately 40-42 Å. The determination of the radial distance of Cys-374 was accomplished by using monobromobimane and *N*-[[(iodoacetyl)amino]ethyl]-5-naphthylamine-1-sulfonate as donors and *N*-[4-[[4-(dimethylamino)phenyl]azo]phenyl]maleimide as acceptor; the results were consistent with a radial coordinate for this residue of 20-25 Å. The effect of myosin subfragment 1 (S1) binding on the radial coordinates of (1) Gln-41, (2) Cys-374, and (3) the nucleotide binding site was also examined. S1 had a small effect on the radial coordinate of Gln-41, increasing it to 44-47 Å. In the two remaining cases the change in the radial coordinate due to the S1 binding was negligible. This finding excludes certain models of the interaction between actin and S1 in which actin monomer rotates by a large angle when subfragment 1 binds to it.

From low-resolution X-ray crystallography and electron microscopy it has been found that the structure of G-actin is bilobar (Suck et al., 1981; Kabsch et al., 1985; Taylor & Amos, 1983; Amos, 1985; Tajima et al., 1983; Egelman & DeRosier, 1983). The N-terminal portion of the molecule is in the smaller lobe whereas the C-terminus is in the larger. The phosphate moiety of the actin-bound nucleotide is located presumably in the interdomain space (Kabsch et al., 1985). While a high-resolution crystallographic structure of G-actin complexes with profilin (Carlsson et al., 1976; Schutt et al., 1985) and DNase[1] (Suck et al., 1984; Kabsch et al., 1985) is slowly emerging, the orientation of the monomer in the thin filament is still an open question.

Numerous attempts have been made to fit the available, low-resolution structure of monomeric actin into the filament [for a review see Egelman (1985)]. This is, of course, only the first step in the filament reconstruction since the difference in conformation between G-actin monomer and F-actin protomer is unknown. To date, however, in spite of efforts by several laboratories, no definite answer to the question of orientation has been obtained.

Besides crystallography and electron microscopy other techniques are helpful in orienting the monomer. Cross-linking

†This work was supported by grants from the National Science Foundation (NSF PCM 8316007 and INT-8414375) and National Institutes of Health Program Project Grant HL-16683. M.F.M. is a Career Investigator of the American Heart Association.
* Address correspondence to this author at the Cardiovascular Research Institute, HSW-841, Box 0524, University of California, San Francisco, CA 94143.

[1] Abbreviations: S1, myosin subfragment 1; 1,5-IAEDNS, *N*-[[(iodoacetyl)amino]ethyl]-5-naphthylamine-1-sulfonate; DABM, *N*-[4-[[4-(dimethylamino)phenyl]azo]phenyl]maleimide; DAB, [[4-(dimethylamino)phenyl]azo]benzene; TNP-ADP, 2′(3′)-*O*-(2,4,6-trinitrophenyl)adenosine 5′-diphosphate; TNP-ATP, 2′(3′)-*O*-(2,4,6-trinitrophenyl)adenosine 5′-triphosphate; ε-ADP, 1,$N^6$-ethenoadenosine 5′-diphosphate; DNC, dansylcadaverine; RHC, rhodamine cadaverine; FLC, fluorescein cadaverine; MBB, monobromobimane; FRET, fluorescence resonance energy transfer; rms, root mean square; DNase, deoxyribonuclease; Tris-HCl, tris(hydroxymethyl)aminomethane hydrochloride; TES, 2-[[tris(hydroxymethyl)methyl]amino]ethanesulfonic acid.

0006-2960/88/0427-4512$01.50/0 

experiments (Knight & Offer, 1978; Elzinga & Phelan, 1984) provided the evidence that Cys-374 is less than 1 nm away from Lys-191 in the adjacent monomer. So far it is the only proximity in the filament obtained from chemical cross-linking.

A potentially powerful method to study the structure of filamentous actin was introduced by Taylor et al. (1981). These authors utilized fluorescence resonance energy transfer (FRET) to measure the distance between equivalent chemical points on different actin protomers. In this approach one should be able to obtain two preparations of actin: donor actin and acceptor actin possessing the same modified amino acid. The extent of FRET is measured for a copolymer of both proteins mixed in controlled proportion. Since the geometry of the actin helix is known, the interchromophore distance obtained from FRET can be related to the *radial* distance of the modified residue. [The radial distance is defined as the distance of the given point to the (imaginary) filament axis.] It is expected that when a number of radial distances are measured, the monomer can be uniquely oriented about the filament axis. However, it is not known how many radial coordinates are required to accomplish a unique orientation of the monomer and what information about *intramolecular* distances within the body is sufficient for such filament reconstruction.

The first radial coordinate measured by this method was Cys-374, which was reported to be located ~35 Å from the axis (Taylor et al., 1981). Subsequently, radial distances of two additional points, viz., Cys-10 and the nucleotide binding site, have been reported (Miki et al., 1986a,b).

The availability of a physical method by which one may, in solution, discover the orientation of actin in the filament leads to the next important question: What is the effect of various actin-binding proteins on the orientation of the monomer in the filament? The ability of actin subunits to rotate has been postulated early on (Hanson, 1967; Huxley et al., 1972). The torsional flexibility of actin has been detected by using both transient absorption probes (Yoshimura et al., 1984) and saturation-transfer electron paramagnetic spectroscopy (Thomas et al., 1979). Oosawa and collaborators (Oosawa, 1983; Yanagida et al., 1984) extensively studied mechanical properties of F-actin and found not only that restricted monomer rotations did occur in the filament but also that these fluctuations could be modulated by the muscle regulatory proteins and heavy meromyosin.

The results of these studies together with the electron microscopic observation of the variable twist in F-actin (Egelman et al., 1982; Stokes & DeRosier, 1987) lead to the conclusion that the torsional flexibility of the thin filament and its modulation by actin-binding protein are naturally occurring and biologically important phenomena related to various functions of actin in muscle and nonmuscle cells. In all these cases the observed or deduced changes in the position of the monomer were relatively small, ranging from 1° to 15°.

Another hypothesis concerning the effect of actin-binding proteins has been presented by Mornet and Ue (1984). They suggested that S1, unlike other proteins, may evert the actin molecule to which it is bound, so that the small domain, normally inaccessible in F-form, becomes exposed to the outside of the filament. Presently there is no way to estimate the expected angular displacement caused by S1 binding.

In this paper we have presented a proof that four distances are necessary to orient actin monomer about the F-filament axis. Using a recently developed method of enzymatic labeling of Gln-41 of actin (Takashi & Kasprzak, 1985, 1987; Takashi, 1988), we have measured a new radial distance required for unambiguous monomer orientation. Then we have examined the effect of S1 binding on three radial coordinates of F-actin: Cys-374, Gln-41, and the nucleotide binding site.

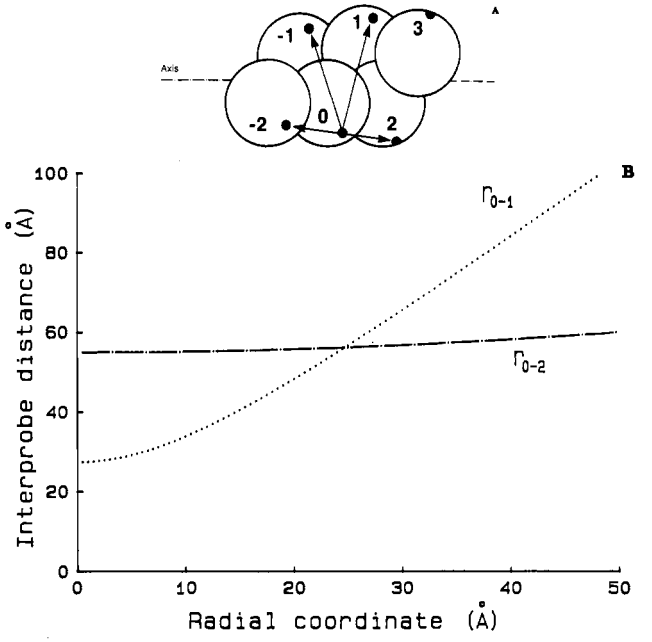


FIGURE 1: (A) Schematic model of the actin filament. Each large dot represents labeled chemical point (donor or acceptor). The arrows show interchromophore distances from actin 0 to four adjacent monomers. (B) Dependence of interprobe distance between two chemical points on the radial distance for these points: (–·–) distance from actin 0 to actin 2 (or –2); (···) interprobe distance from actin 0 to actin 1 (or –1). The distances were calculated from eq 4.

## THEORY

*Positioning a Rigid Body Relative to an Axis.* FRET measurements can only produce scalar distances, so it is necessary at the outset to show that the estimation of certain distances allows one to infer the orientation of the actin monomer in the helical F-filament or—more generally—the positioning of a rigid body relative to an axis. It turns out (see Appendix A) that within symmetry limits two kinds of distances have to be estimated—four perpendicular distances from points in the body to the axis (here these are called "radial" distances) and six distances between the points in the body.

*Fluorescence Decay of Probes Bound to the Actin Filament in the Presence of Energy Transfer.* We consider several actin monomers assembled into the filament (Figure 1A). The geometry of the filament is known; each successive actin subunit is related to the previous one by a rotation of 166° and a translation in the direction parallel to the filament axis of 27.5 Å (Squire, 1981). The dependence of the distance between two equivalent chemical points (in angstroms) on the filament on the radial distance of that point is given by

$$r_{0\to k} = [2n_A^2[1 - \cos(166k)] + (27.5k)^2]^{1/2} \quad (1)$$

where $r_{0\to k}$ is the interprobe distance between monomer 0 and monomer $k$ and $r_A$ is the radial distance. Since FRET is inversely proportional to the sixth power of the distance, simple calculation shows that FRET may take place between the donor actin and one or more of the four adjacent molecules (1, 2, –1, and –2 in Figure 1A). The distances to actins located further away, e.g., 3 or –3, are too long for a significant transfer to occur.

We have computed the interprobe distance from actin 0 to actins 2 (or –2) and to actins 1 (or –1) as a function of the radial distance (Figure 1B). It is clear that FRET depends predominantly on the distance across the filament because

interprobe distances to actins located in the same strand (2 and −2) are rather constant (Figure 1B).

A mole fraction, $x_A$, of actin monomers is acceptor-labeled, another fraction is donor-labeled, and still another is unlabeled. Since both labeling and copolymerization are random, $x_A$ may be taken as the probability that a chosen protomer is acceptor-labeled and $1-x_A$ that it is either donor-labeled or unlabeled (in either case it is unable to receive transfer). A particular donor "sees" two potential transfer sites at distance $r(\pm 1)$ and two others at $r(\pm 2)$. The labeling status of these sites is a matter of chance. However, we can calculate $p(u|v)$, the probability that there be $u$ acceptor-labeled sites at $r(\pm 1)$ and $v$ sites at $r(\pm 2)$, with $u, v = 0$, 1, and 2. If the probabilities of labeling and not labeling a site at $r(\pm 1)$ are $p$ and $q$, and at $r(\pm 2)$ they are $P$ and $Q$, then the $p(u|v)$ of nine possible ways of distributing label among the two distance classes are conveniently generated by expanding $(p + q)^2(P + Q)^2$. In our case $P = p = x_A$ and $Q = q = 1 - x_A$, so the probabilities[2] are like those obtained by expanding $(p + q)^4$.

We next consider the effect of acceptor distribution around a donor on the transfer rate constant, $k^T$. For parallel, pairwise transfer, the resonance-transfer rate constant to multiple acceptors is proportional to the sum of $(R_0/r_i)^6$ terms, each term corresponding to the transfer between the donor and a particular acceptor (Eisenthal & Siegel, 1964). With $u$ acceptors at $r(\pm 1)$ and $v$ acceptors at $r(\pm 2)$ we can write

$$k^T_{uv} = \left(\frac{1}{\tau_0}\right)\left[u\left(\frac{R_0}{r_1}\right)^6 + v\left(\frac{R_0}{r_2}\right)^6\right] = \left(\frac{1}{\tau_0}\right)S_{uv} \qquad (2)$$

where $S_{uv}$ denotes the expression in square brackets, and $u$, $v = 1$, 2, and 3.

The average efficiency of energy transfer $\langle E\rangle$ in such systems is

$$\langle E\rangle = \sum_{u,v}\left[p(u|v)\frac{k^T_{uv}}{1/\tau_0 + k^T_{uv}}\right] = \sum_{u,v}\left[p(u|v)\frac{S_{uv}}{1 + S_{uv}}\right] \qquad (3)$$

Knowing $R_0$ and using eq 3, one can construct a family of curves, each corresponding to the transfer efficiency as a function of $x_A$ with the radial distance held constant—to find out which of the curves fits the experimental data best (see Figure 4). We assume that a procedure like this was used to determine radial distances from steady-state measurements (Taylor et al., 1981; Miki et al., 1986a,b). When lifetimes were employed (Taylor et al., 1981), the extent of transfer was calculated presumably from their average values. We describe below how time-resolved spectroscopy can be employed to obtain the value of the radial coordinate, when FRET takes place in the actin filament.

Fluorescence intensity $F(t)$ after a $\delta$-function excitation pulse is described by

$$\langle F(t)/F(0)\rangle = \sum_{u,v}p(u|v)\sum_{j=1}^{m}\alpha_j \exp[-(1/\tau_{0j} + k^T_{uv})t]$$
$$= \sum_{u,v}p(u|v)\sum_{j=1}^{m}\alpha_j \exp\left[-\frac{t}{\tau_{0j}}(1 + S_{uv})\right] \qquad (4)$$

where $\alpha_j$ and $\tau_{0j}$ denote the preexponential factor and the corresponding lifetime for the $j$th component of the decay and $m$ is the number of components in the decay. Similar equations were obtained by Grinvald et al. (1972) in order to obtain distribution of end-to-end distances of oligopeptides in solution from FRET, and by Fung and Stryer (1978), who studied fluorescence decay of dansyl- and eosin-labeled phospholipids in synthetic membrane vesicles.

It is clear from eq 4 that when a monoexponential donor is placed in the filament together with acceptors, it will obey a complex, multiexponential decay law. Since there are nine different configurations of acceptors around each donor (eight quenched configurations and one unquenched), the fluorescence decay of the donor will consist of nine decay components. Our experimental precision is far too low to recover all the parameters of such decay components. Also, because the contributions of these components to the average lifetime are weighted by their fractional fluorescence intensities (Badley & Teale, 1969), there is no simple relation between $E_T$ and $\langle\tau\rangle_{av}/\tau_0$. However, as we show in the Appendix B, the same $\langle E\rangle$ defined in eq 3 can be obtained from a simple integration of the normalized decay curve of the donors, measured in the presence and absence of the acceptors. This procedure yields accurate results only if the Förster critical distance, $R_0$, is identical for all components. On the other hand, the quantities in the equation for $R_0$ are usually determined from steady-state spectroscopy, averaging possible differences in quantum yield, overlap integrals, etc., for different lifetime components. While such averaging may result in a modest error in $\langle E\rangle$, one has to accept that in cases in which the $R_0$ is not the same for components not only is $1 - A/A_0$ (where $A$ and $A_0$ denote the areas under normalized decay curve in the presence and absence of FRET, respectively) an approximation of $\langle E\rangle$ but also eq 3 should be modified to take into account heterogeneity in $R_0$.

Time-resolved spectroscopy was used in this paper to determine $\langle E\rangle$ because there are clear advantages of using this technique over steady-state fluorometry. One of them is the insensitivity of the former to trivial reabsorption, static quenching, and other effects not related to nonradiative energy transfer. Another useful characteristic of the lifetime measurements is their independence of the absolute concentration of the fluorophores. The third, and probably the most important, advantage is the possibility of verifying that the fluorescence of the donor indeed decays in the way predicted by the model. This can be utilized, for example, to test whether the donor actin and acceptor actin form a *random* copolymer. Further details are given under Results.

Finally, we have included in the equations describing FRET a known property of the actin filament—its variable twist. Following Egelman and DeRosier (1982) we have assumed that the angular disorder in the filament is a Gaussian distribution with a rms deviation of 10°. We have introduced the variable twist to the FRET equations by computing the "equivalent distance", $r_e$, defined as the distance at which a single molecular of the acceptor would result in the same FRET as a set of molecules that are rotated by an angle which is normally distributed around the 166° value with rms of 10°:

$$\int_{-\infty}^{+\infty}\left[P_G(r_k,r_0,w)\frac{(R_0/r_k)^6}{1 + (R_0/r_k)^6}\right]dr_k = \frac{(R_0/r_{ek})^6}{1 + (R_0/r_{ek})^6} \qquad (5)$$

$P_G(r_k,r_0,w)$ denotes the probability that the donor–acceptor distance lies between $r$ and $r + dr$, $r_0$ is the most probable distance, and $w$ is the rms of the distribution. By solution of eq 5 for $r_{ek}$, the equivalent distance is obtained directly. Figure

[2] These probabilities are as follows: $p(0|0) = (1 - x_A)^4$, $p(1|0) = 2x_A(1 - x_A)^3$, $p(2|0) = x_A^2(1 - x_A)^2$, $p(0|1) = 2x_A(1 - x_A)^3$, $p(1|1) = 4x_A^2(1 - x_A)^2$, $p(2|1) = 2x_A^3(1 - x_A)$, $p(0|2) = 4x_A^2(1 - x_A)^2$, $p(1|2) = 2x_A^3(1 - x_A)$, and $p(2|2) = x_A^4$.

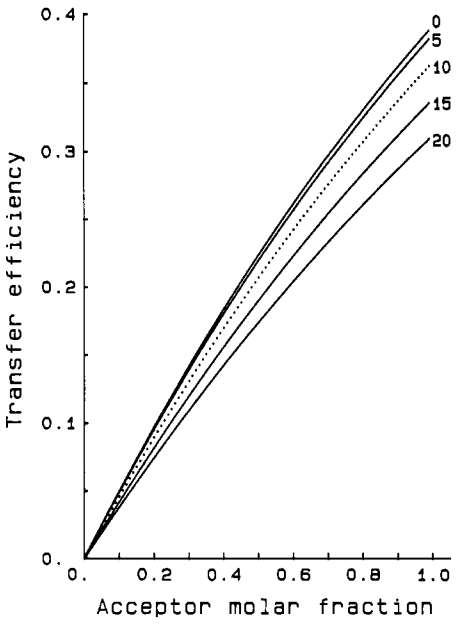


FIGURE 2: Effect of the angular disorder of actin on the fluorescence energy transfer in the filament. The numbers next to the curves indicate the assumed value of the rms for fluctuation of the angle between monomers. Gaussian distribution of these fluctuations was assumed (Egelman & DeRosier, 1982).

2 shows the effect of the filament disorder on the computed FRET in the filament. Generally, the variable twist of actin has a small but not a negligible effect on the FRET in the filament and, if completely disregarded, leads to a slight overestimation of the measured distances (see also Figure 4).

## Materials and Methods

*Chemicals.* The following chemicals were purchased from Molecular Probes, Inc. (Eugene, OR), and used without purification: DABM, 1,5-IAEDNS, DNC, RHC, FLC, and $\epsilon$-ATP. TNP-ATP from Molecular Probes was further purified chromatographically by the method of Hiratsuka and Uchida (1973). MBB was obtained from Calbiochem. Sources of other chemicals were listed earlier (Takashi & Kasprzak, 1987).

*Proteins.* Rabbit skeletal muscle actin was prepared according to Spudich and Watt (1971). S1 from rabbit back muscle was obtained by the method of Weeds and Taylor (1975). Transglutaminase was purified from fresh guinea pig livers (Connellan et al., 1971). The concentration of unlabeled G-actin was measured spectrophotometrically by using $A^{1\%}_{290nm} = 6.30$ or $A^{1\%}_{280\ nm} = 11.1$ (Houk & Ue, 1974); for labeled actin the Lowry method was employed. In some cases the concentration of a derivatized protein was assessed from absorbance at 280 nm. In such cases the protein absorption was corrected for the absorption of the label at 280 nm as described earlier (Takashi & Kasprzak, 1987). The following extinction coefficients (in $M^{-1}$ $cm^{-1}$) for the labeled proteins were assumed: MBB, $\epsilon_{390} = 4.7 \times 10^3$ (Kosower & Panzhenchensky, 1980); DAB, $\epsilon_{460} = 2.48 \times 10^4$ (Tao et al., 1983); 1,5-IAEDNS, $\epsilon_{336} = 6.0 \times 10^3$ (Hudson & Weber, 1983); FLC, $\epsilon_{493} = 7.55 \times 10^4$ (Lorand et al., 1983); RHC, $\epsilon_{555} = 5.68 \times 10^4$ (Takashi, unpublished results); DNC, $\epsilon_{326} = 4.64 \times 10^3$ (Lorand et al., 1968); TNP-ADP, $\epsilon_{408} = 2.64 \times 10^4$ (Hiratsuka & Uchida, 1973).

*Preparation of Fluorescently Labeled Actin.* The labeling reagents were dissolved in dimethylformamide or acetonitrile at concentrations of 10–50 mM. Aliquots of the stock solutions were added to the actin. The final concentration of the organic solvent was always below 0.6%.

*Labeling of actin with MBB* was carried out as follows: G-Actin at a concentration of 50 $\mu$M was incubated with a 5-fold molar excess of MBB in a buffered solution containing 2 mM Tris-HCl, pH 8.0, 0.2 mM $CaCl_2$, and 0.2 mM ATP for 2 h at 4 °C. The reaction was terminated by an excess of dithiothreitol, and the unreacted reagent was removed by Sephadex G-25 chromatography.

*DABM–actin* was prepared by the procedure of Tao et al. (1983) with a slight modification. G-Actin (107 $\mu$M) was incubated with a 1.3-fold molar excess of DABM in a solution containing 2 mM Tris-HCl, pH 8.0, 0.2 mM $CaCl_2$, and 0.2 mM ATP for 17 h on ice. The reaction was quenched by addition of excess dithiothreitol, and actin solution was passed down a Sephadex G-25 column to remove unreacted DABM.

*1,5-IAEDNS–actin* was prepared following a procedure similar to that of Tao and Cho (1979). G-Actin at concentration of 50 $\mu$M was reacted with a 10-fold molar excess of 1,5-IAEDNS in a buffer containing 2 mM Tris-HCl, pH 8.0, 0.2 mM $CaCl_2$, and 0.2 mM ATP for 15–17 h at 4 °C in the dark.

*Labeling of Gln-41 with DNC, RHC, and FLC.* Three fluorescent derivatives, viz., dansylcadaverine, rhodamine cadaverine, and fluorescein cadaverine were used. Enzymatic modification of Gln-41 with these labels was performed as described previously (Takashi & Kasprzak, 1987; Takashi, 1988).

*Exchanging Actin-Bound ADP into Chromophoric Nucleotides.* F-Actin containing bound $\epsilon$-ADP was prepared essentially by the methods of Miki and Wahl (1984) and Miki et al. (1986b). Polymerization of G-actin–ATP at a concentration of 50–80 $\mu$M was induced by adding 50 mM NaCl at 4 °C and was allowed to proceed for 2 h at 25 °C. The F-actin thus obtained was centrifuged at 160000*g* for 45 min, and the pellet (at a concentration of 50–80 $\mu$M) was gently homogenized with and dissolved in a buffer containing 1 mM Tris-HCl, pH 8.0, and 0.4 mM $\epsilon$-ATP at 4 °C. The resulting solution of actin was dialyzed against 1 mM Tris-HCl, pH 8.0, containing 60 $\mu$M $\epsilon$-ATP overnight and centrifuged at 130000*g* for 60 min. $\epsilon$-ATP–G-actin (50–80 $\mu$M) in 1 mM Tris-HCl, pH 8.0, was treated with $^1/_{20}$ volume of Dowex 1 (Asakura, 1961) at 0 °C for 10 min and passed through a 0.45-$\mu$m Millipore membrane to remove the resin. $\epsilon$-ATP–G-actin was immediately polymerized into $\epsilon$-ADP–F-actin by the addition of 0.1 M NaCl and 10 mM sodium phosphate, pH 7.0 at 25 °C.

*TNP-ADP was partially exchanged into $\epsilon$-ADP–F-actin* by the procedure of Miki et al. (1986b). A 5–20-fold molar excess of TNP-ATP was added to $\epsilon$-ADP–F-actin in a buffer containing 0.1 M NaCl and 10 mM sodium phosphate, pH 7.0, and the solutions were sonicated by using a Kontes cell disrupter at the maximum power setting, on ice, for a total time of 150 s. The resulting solutions were then centrifuged at 160000*g* for 45 min so as to remove unbound TNP-ATP. The actin pellets were redissolved in the above buffer and recentrifuged. The last step was repeated until the amount of free TNP-ATP became negligible. Finally, the pellets were dissolved in 0.1 M KCl, 10 mM potassium phosphate, pH 7.0, and 1 mM $MgCl_2$, and the F-actin solutions were used for FRET measurements.

*The copolymers of donor and acceptor actin* for fluorescence measurements were prepared as follows: Aliquots of freshly prepared donor and acceptor G-actin were mixed in a required proportion, and if necessary, unlabeled actin was added. The polymerization of actin at concentrations of 40–50 $\mu$M was initiated by adding KCl to 50 mM and $MgCl_2$ to 1 mM at

Table I: Stoichiometry of Labeling and S1 Binding for Copolymers of Modified Actin[a]

| sample | acceptor molar fraction | actin total (μM) | actin unpolymerized (μM) | S1 total (μM) | S1 unpolymerized (μM) | actin + S1 in pellet[b] (μM) | [S1]/[actin] |
|---|---|---|---|---|---|---|---|
| DNC–RHC | 0.331 | 10.0 | 0.327 | 9.02 | 8.60 | 0.260 | 0.926 |
| DNC–RHC | 0.510 | 10.0 | 0.333 | 9.02 | 8.60 | 0.148 | 0.619 |
| DNC–RHC | 0.714 | 10.0 | 0.341 | 9.02 | 8.60 | 0.246 | 0.899 |
| DNC–FLC | 0.373 | 10.0 | 0.460 | 9.02 | 8.60 | 0.339 | 0.918 |
| DNC–FLC | 0.522 | 10.0 | 0.517 | 14.5 | 14.22 | 0.331 | 0.839 |
| MBB–DABM | 0.491 | 4.56 | 4.2 | nd | 3.88 | 0.363 | 0.938 |
| MBB–DABM | 0.884 | 4.56 | 4.2 | nd | 3.88 | 0.465 | 0.990 |
| 1,5-IAEDNS–DABM | 0.491 | 4.56 | 4.2 | nd | 3.88 | 0.163 | 0.884 |
| control | 0 | | nd[c] | 4.2 | 3.88 | 0.135 | 0.944 |
| control | 0 | 10.0 | 0.400 | 11.0 | 10.0 | 0.079 | 0.794 |

[a] The extent of S1 binding to F-actin was determined by the method of Katoh et al. (1984). [b] The ratio of [S1]/[actin] in the pellet after centrifugation for 60 min at 130000*g*. The buffer used was 10 mM TES, pH 7.5, 50 mM KCl, and 1 mM $MgCl_2$, 20 °C. [c] nd, not determined.

Table II: Spectroscopic Parameters of Fluorescent Labels Bound to F-Actin

| probe | actin residue | $\alpha_1$ | $\tau_1$[a] (ns) | $\alpha_2$ | $\tau_2$[a] (ns) | $Q$ | $r_x$ | $r_0$ | $d_x$ |
|---|---|---|---|---|---|---|---|---|---|
| DNC[b,c] | Gln-41 | 0.52 | 9.78 | 0.48 | 22.33 | 0.36 | 0.287 | 0.351 | 0.904 |
| RHC[d] | Gln-41 | | | nd[m] | | | 0.196 | 0.356 | 0.742 |
| FLC[e] | Gln-41 | | | nd | | | 0.217 | 0.341 | 0.797 |
| MBB[f] | Cys-374 | 0.55 | 7.90 | 0.45 | 17.60 | 0.27 | 0.288 | 0.339 | 0.913 |
| 1,5-IAEDNS[g] | Cys-374 | 0.42 | 15.39 | 0.58 | 21.64 | 0.63[h] | 0.340[i] | 0.376[i] | 0.951 |
| ε-ADP[j] | N site | 1.0 | 30.7 | | | 0.75[k] | 0.234[k] | 0.308[l] | 0.872 |

[a] Unquenched lifetimes. [b] Excited through a combination of UG1 + UG11 filters; $\lambda_{em}$ = 486 nm. [c] Takashi & Kasprzak, 1987. [d] $\lambda_{ex}$ = 530 nm, $\lambda_{em}$ = 589 nm; rhodamine cadaverine actin (10 μM), 20 °C; in the presence of 10 μM S1, $r_x$ = 0.1923. [e] $\lambda_{ex}$ = 486 nm, $\lambda_{em}$ = 546 nm; fluorescein cadaverine actin (10 μM), 20 °C; in the presence of 10 μM S1, $r_x$ = 0.2242. [f] A. A. Kasprzak, unpublished results. [g] $\lambda_{ex}$ = 380 nm, $\lambda_{em}$ = 467 nm, 20 °C. [h] Takashi, 1979. [i] Torgerson & Morales, 1984. [j] $\lambda_{ex}$ = 330 nm; emission was observed through a combination of BG3 + KV389 + KG3 filters. [k] Miki & Wahl, 1984. [l] Secrist et al., 1972. [m] nd, not determined.

4 °C. The polymerization was allowed to proceed for 2 h at 25 °C and then overnight at 4 °C. The polymerized actin was diluted to a desired concentration in a buffer containing 50 mM KCl, 1 mM $MgCl_2$, 10 mM TES, pH 7.5, and 0.5 mM dithiothreitol. Actin samples were incubated for at least 30 min at room temperature in this buffer prior to fluorescence measurements.

*Steady-state fluorescence and absorption measurements* were performed on an SLM 8000 fluorometer and a Cary 118 spectrophotometer, respectively (Takashi & Kasprzak, 1987).

*Fluorescence lifetimes* were measured by using a single-photon counting instrument whose optical components were purchased from PRA, Inc. (London, Ontario, Canada), and the associated electronics and data collection system were from Ortec, Inc. (Oak Ridge, TN). The nanosecond lamp (Model 510B from PRA) was filled with deuterium at 0.5 atm. The data collection system consisted of a multiplexed Model 918A multichannel buffer (Ortec) interfaced to an IBM PC computer. The 918 software was purchased from Ortec. A section of the MCB storage area, typically 2048 channels, was first transferred to the IBM computer and subsequently to a Micro-Vax II computer (Digital Equipment Corp.) for analysis. Deconvolution of the fluorescence decay was accomplished by using a nonlinear least-squares analysis program (Badea & Brand, 1975; Grinvald & Steinberg, 1974).

*The Förster critical distances* were calculated as described earlier (Takashi & Kasprzak, 1987). To compute the values of depolarization factors for the Dale–Eisinger analysis, the anisotropy of a nonimmobilized label attached to F-actin, $r_x$, was measured by using the steady-state fluorometer (Takashi & Kasprzak, 1987). A second measurement was made by using the same dye, free or conjugated with β-mercaptoethanol, in 99.9% glycerol at −21 °C, yielding a value of $r_0$. The axial depolarization factor $d_x$ was computed from the equation:

$$d_x = (r_x/r_0)^{1/2} \quad (6)$$

The values of $\kappa_{min}^2$ and $\kappa_{max}^2$ were calculated as described by Dale et al. (1979):

$$\kappa_{min}^2 = \tfrac{2}{3}[1 - (d_D + d_A)/2] \quad (7)$$

$$\kappa_{max}^2 = \tfrac{2}{3}(1 + d_D + d_A + 3d_D d_A) \quad (8)$$

where $d_D$ and $d_A$ are axial depolarization factors for the donor and acceptor, respectively.

## Results

We have prepared a number of labeled F-actin derivatives, each containing copolymerized donor, acceptor, and unlabeled protein. These preparations, later used for FRET measurements, were first characterized biochemically by measuring the labeling stoichiometry and the amount of unpolymerized actin that remained in solution after centrifugation (Table I). These measurements were repeated in the presence of S1, and the ratio of [S1] to [actin] in the pellet was monitored. The results presented in Table I indicate that in all cases we have dealt with specifically labeled actin, capable of polymerizing and binding S1 with affinity similar to the native protein. Spectroscopic properties of the fluorescent probes used in this paper are summarized in Table II. Table III shows the overlap integrals and Förster critical distances. The results of FRET measurements are presented in Table IV.

*Radial Distance of Gln-41.* Two donor–acceptor pairs have been employed to measure the radial distance of Gln-41: dansylvadaverine–rhodamine cadaverine and dansylcadaverine–fluorescein cadaverine. All three probes were enzymatically attached to Gln-41 according to the method described elsewhere (Takashi & Kasprzak, 1987; Takashi, 1988). The labeling stoichiometry (before copolymerization) was 0.946, 0.833, and 0.745 for DNC, RHC, and FLC, respectively.

The use of the time-resolved spectroscopy enabled us to check independently our model of FRET in the filament. In

Table III: Overlap Integrals and Förster Critical Distances

| donor | acceptor | $J$ ($nm^4$ $M^{-1}$ $cm^{-1}$) | $\kappa^2$(min) | $\kappa^2$(max) | $R_0$(min) (Å) | $R_0(^2/_3)$ (Å) | $R_0$(max) (Å) |
|---|---|---|---|---|---|---|---|
| DNC | RHC | $2.07 \times 10^{15}$ | 0.118 | 3.106 | 35.5 | 47.4 | 61.3 |
| DNC | FLC | $8.78 \times 10^{14}$ | 0.100 | 3.242 | 29.9 | 41.1 | 53.5 |
| MBB | DABM[a] | $7.70 \times 10^{14}$ | 0.029 | 3.769 | 22.7 | 38.3 | 51.2 |
| 1,5-IAEDNS | DABM[a] | $6.42 \times 10^{14}$ | 0.016 | 3.869 | 23.1 | 42.8 | 57.4 |
| $\epsilon$-ADP | TNP-ADP[a] | $5.99 \times 10^{14}$ | 0.043 | 3.659 | 27.6 | 43.6 | 57.9 |

[a] For nonfluorescencent acceptors $d_x$ of 1 was assumed.

Table IV: Energy Transfer between Probes Bound to F-Actin Filament[a]

| donor | acceptor | S1 | $x_A$ | $E_1$[b] (%) | $r_A$ (Å) |
|---|---|---|---|---|---|
| DNC[c] | RHC | – | 0.331 | 13.9 | 40 |
| DNC | RHC | + | 0.331 | 11.3 | 47 |
| DNC | RHC | – | 0.510 | 20.0 | 42 |
| DNC | RHC | + | 0.510 | 19.4 | 44 |
| DNC | RHC | ++[d] | 0.510 | 19.9 | 44 |
| DNC | RHC | – | 0.714 | 28.0 | 40 |
| DNC | RHC | + | 0.714 | 25.4 | 45 |
| DNC | FLC | – | 0.374 | 9.3 | |
| DNC | FLC | + | 0.374 | 38.2 | |
| DNC | FLC | – | 0.522 | 39.6 | |
| DNC | FLC | + | 0.522 | 15.8 | |
| MBB[c] | DABM | – | 0.491 | 25.3 | 20 |
| MBB | DABM | + | 0.491 | 25.0 | 20 |
| MBB | DABM | – | 0.884 | 38.0 | 22 |
| MBB | DABM | + | 0.884 | 39.3 | 22 |
| 1,5-IAEDNS[c] | DABM | – | 0.491 | 24.9 | 25 |
| 1,5-IAEDNS | DABM | + | 0.491 | 24.6 | 25 |
| $\epsilon$-ADP[c,e] | TNP-ADP | – | 0.30 | 14.5 | 30 |
| $\epsilon$-ADP | TNP-ADP | + | 0.30 | 13.1 | 30 |
| $\epsilon$-ADP | TNP-ADP | – | 0.45 | 17.8 | 29 |
| $\epsilon$-ADP | TNP-ADP | + | 0.45 | 18.3 | 29 |

[a] DNC, RHC, and FLC were conjugated to Gln-41; MBB, 1,5-IAEDNS, and DABM were attached to Cys-374; $\epsilon$-ADP and TNP-ADP were bound to the nucleotide binding site of F-actin. [b] Computed by integration. [c] Spectroscopic data for unquenched donors are given in Table II. [d] The concentration of S1 has been increased twice (to 17.7 μM). [e] Total actin concentration was 10.6 μM; when S1 was present, its concentration was 11 μM.

order to do so, we have obtained decay parameters (preexponential factors and lifetimes) for the unquenched donors incorporated into F-actin filament. Using these parameters and the radial distance obtained from Figure 4, we have attempted to reconstruct the *time course* of the fluorescence decay convoluted with the lamp profile, in the presence of a known amount of acceptor (Figure 3). A slight divergence from the fit in Figure 3 may indicate that a fraction of acceptors is nonrandomly distributed in the filament or that there are distortions of the filament structure caused by labeling. Nevertheless, the overall agreement between the computed and experimental curves in Figure 3 is good, confirming that our model of FRET in the filament is applicable.

For the DNC–RHC pair the results in the absence of S1 were consistent with a radial coordinate of the dansyl chromophore of 40–42 Å (Table IV and Figure 4). When S1 was present, there was a slight drop in the transfer efficiency (Table IV). This may be interpreted as a small increase in the radial coordinate of the chromophore attached to Gln-41 of actin, to 44–47 Å. The concentration of G-actin in the samples used for fluorescence studies was measured as described under Materials and Methods, and as shown in Table I, the amount of unsedimentable material was found to be small. It was also demonstrated that the concentration of S1 was sufficient to saturate F-actin because when more S1 has been added to the already "decorated" actin filament no further change in the

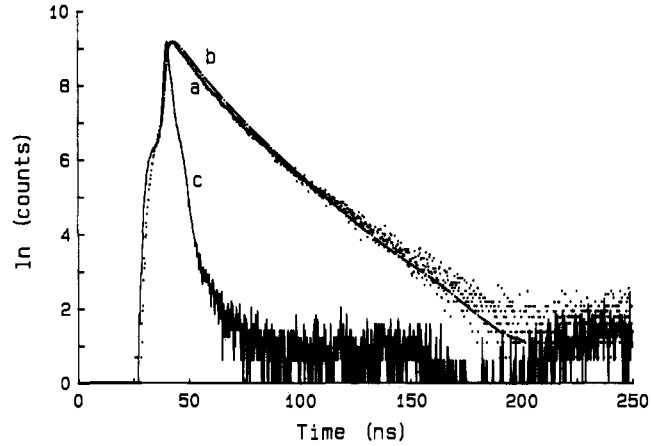


FIGURE 3: Reconstitution of nanosecond kinetics of the fluorescence decay in the presence of energy transfer in the F-actin filament. Nanosecond decay kinetics of DNC–F-actin in the absence of acceptors was found to consist of two components, $\alpha_1 = 0.52$, $\tau_1 = 9.78$ ns, $\alpha_2 = 0.48$, and $\tau_2 = 22.34$ ns. These values were used to simulate the decay convoluted with the lamp profile in the presence of RHC at $x_A = 0.5$ and to compare the computed curve (b) with the experimentally observed fluorescence decay at the same acceptor concentration (a). The solid, noisy line (c) is the lamp profile.

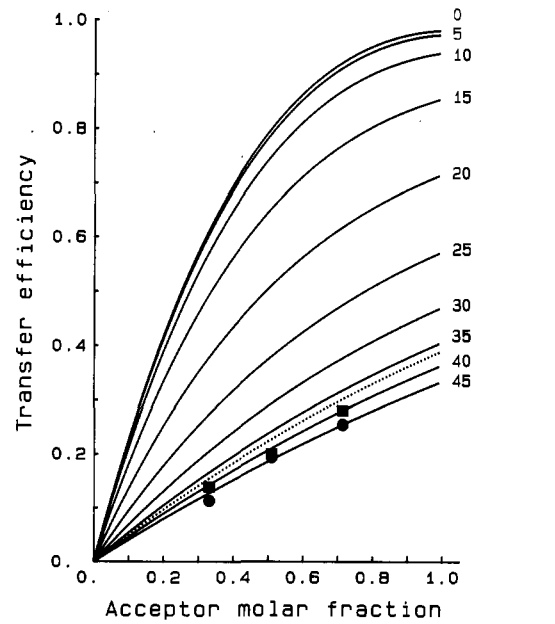


FIGURE 4: Fluorescence energy transfer efficiency in the actin filament plotted as a function of the molar fraction of the acceptor for the copolymerized DNC– and RHC–actin. The numbers next to the curves indicate the assumed values of the radial distance (in angstroms). The dotted line was computed by assuming $r_A = 40$ Å and an rms for the angular distribution of actin twist of 0°; for the other lines, rms = 10° was assumed. Experimental values of $\langle E \rangle$ (●) in the absence of S1 and (■) in the presence of saturating S1 concentration.

efficiency of transfer was seen (Table IV).

The depolarization factors, collected in Table II, indicate that all three probes (DNC, RHC, and FLC) rotate relatively

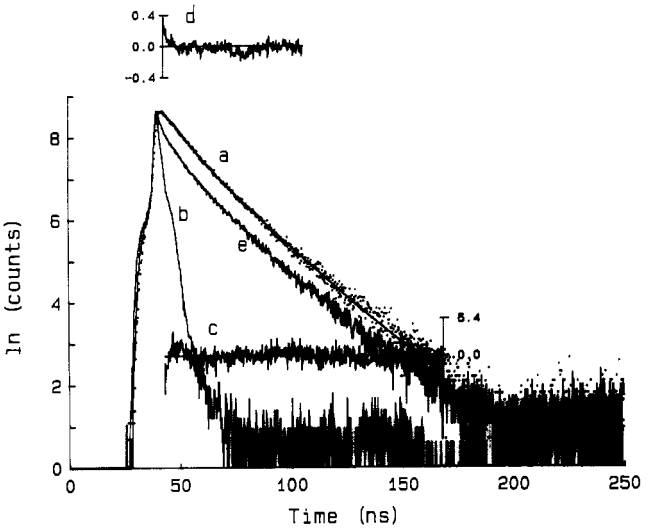


FIGURE 5: Effect of S1 binding on nanosecond decay kinetics of copolymerized DNC- and FLC-actin (10 $\mu$M) at an acceptor molar fraction of 0.374. (a) Dots represent experimentally obtained points. The curve drawn through the data was computed by least-squares analysis with the following parameters: $\alpha_1 = 0.28$, $\tau_1 = 1.19$ ns, $\alpha_2 = 0.28$, $\tau_2 = 10.17$ ns, $\alpha_3 = 0.22$, $\tau_3 = 21.48$ ns, $\chi^2 = 1.30$; residuals (c) and autocorrelation (d) are also shown. (e) Same curve as (a) but in the presence of a saturating concentration of S1; (b) is the lamp profile. The samples were excited through a combination of UG1 + UG11 filters; emission was monitored at 467 nm.

freely, thus reducing the uncertainty of the measured distances. As explained under Discussion, the limits of $R_0$ in Table III are still too wide because they do not take into account that, in the filament, FRET occurs to more than one acceptor.

In contrast to the DNC–RHC pair, FRET between DNC and FLC could not be interpreted in a simple way. In the absence of S1 the lifetimes of DNC at mole fractions of FLC of 0, 0.37, and 0.52 were 17.8, 16.7, and 14.1 ns, respectively. FRET, under these condition, is consistent with a radial coordinate for DNC in the range of 30–35 Å (Table IV), in partial agreement with the previous DNC–RHC pair. The presence of S1 dramatically changes the shape of the decay curves: the early portion of the decay, at short times after the excitation, becomes very steep (Figure 5). There is also some internal inconsistency with this D–A pair: for example, at higher molar ratio of the acceptor the efficiency seems to be lower (Table IV). This probably indicates that the model of FRET in the filament is not applicable to this case. From several control experiments aimed at eliminating trivial reasons for the observed decay pattern we have found that S1 has little influence on the fluorescence properties of FLC–actin and that the shape of the decay was not caused by an increase in turbidity of the solution upon addition of S1.

Computer simulations employing eq 4 have indicated that similarity to the DNC–FLC decay kinetics is expected when an extremely wide distribution of distances is generated. Such a distribution could occur because the monomer orientation or its conformation has been altered when S1 bound to F-actin, or because the dye, being attached to the protein by a long and flexible link, could attain many positions corresponding to various interprobe distances and S1 changed this distribution. We favor the latter hypothesis for two reasons: First, the distortion of the decay pattern caused by S1 binding has not been observed for rhodamine cadaverine attached to the same actin residue. Second, it is known that fluorescein derivatives possess several ionizable groups and their spectral properties are extremely sensitive to the environmental conditions (Babcock, 1983). We have reported previously that S1 has a small effect on the lifetime of the dansyl chromophores in the S1–DNC–actin rigor complex. It is therefore possible that with a different probe this interaction becomes strong and that S1 changes the position of the conjugated chromophore.

*Radial Distance of Cys-374.* To measure the radial distance of Cys-374, we have used two donor–acceptor pairs: MBB–DABM and 1,5-IAEDNS–DAB. Monobromobimane is the smallest of the probes used here: Only one methylene group separates the sulfur of cysteine from the chromophoric ring system of the dye (Kosower et al., 1972). The dye appears to modify a single cysteine on the 33-kDa "core" portion of actin. The stoichiometry was 1.17 mol/mol. For DABM the stoichiometry was found to be 0.982 mol/mol. Considering the known specificity of the probes for thiols and the reactivity of Cys-374, there is little doubt that this cysteine residue of actin underwent modification. The third probe, 1,5-IAEDNS, is known to bind exclusively to Cys-374.

For each of the labels the kinetics of the fluorescence decay were studied for the unquenched dye and for the dye in the presence of acceptors (Table IV). The efficiency of transfer was relatively high, even at $x_A \sim 0.5$, indicating that the *interprobe* distances were in the same range as $R_0$ for the labels used. A good agreement was obtained between the values of $r_A$ for these two probes. As shown in Table IV, the radial distance of Cys-374 appears to be 20–25 Å. S1 has no effect on the radial coordinate of this residue.

*Radial Distance of the Nucleotide Binding Site.* The determination of the radial distance of the nucleotide binding site requires that two spectrally complementary nucleotide analogues be available and that the ADP normally present at this site could be exchanged in one preparation into the donor and in the other into the acceptor nucleotide. There are two nucleotide pairs suitable for such work: $\epsilon$-ADP and TNP-ADP and formycin A 5′-triphosphate and $\epsilon$-ADP. Because of the higher value of the overlap integral, the former pair was used to measure FRET between the nucleotide base of $\epsilon$-ADP and the ribose-attached trinitrophenyl moiety of TNP-ADP. There is no flexible link between the chromophore and the protein. However, the TNP moiety and $\epsilon$-adenosine are at different positions of the nucleotide, so in this case the $r_A$ is determined with a slightly lower accuracy. In the absence of S1 the radial distance of the nucleotide binding site was 29–30 Å, slightly higher than the previously reported value obtained from steady-state measurements, 25 Å (Miki et al., 1986b). The decay kinetics of the $\epsilon$-ADP fluorescence did not change when S1 at saturating concentration was added to the F-actin solution (Table IV).

## Discussion

The orientation of the actin monomer in the filament is important in understanding the biological function of this protein. It is the filamentous form of actin that interacts not only with myosin but also with the muscle regulatory system (tropomyosin, troponin). Various investigations directed toward orienting actin in the filament have not, so far, reached a satisfactory conclusion. Using the method of radial distance measurements, we have measured the radial coordinates of Cys-374, the nucleotide binding site, and Gln-41 in F-actin and have examined the effect of S1 on these radial coordinates.

Theoretical considerations (see Appendix A) indicate that a minimum of four radial distances must be measured in order to position actin in the filament assembly. Hence, the present work is a step toward completion of these measurements. Besides Gln-41 three other radial coordinates have been reported: Cys-374, the nucleotide binding sites, and Cys-10.

However, there is an uncertainty as to whether Cys-10 can be specifically labeled by the method used so far. The proximity of Cys-374 and Lys-191 can be used to eliminate possible ambiguities of the monomer orientation, resulting from nonspecific labeling, inaccurate distance measurements, uncertainty of the orientation factor, etc. Nevertheless, positioning of the monomer by this method is not yet at hand, since certain *intramonomer* distances are still missing.

Although we can measure radii of points in the filament, we cannot assign a radius to the center of mass for a lobe or domain unless many points belonging to that domain have known radial coordinates. Thus, the long-debated question, which domain (N or C terminal) has the greater radius, cannot be answered from the presently available data. The filament has a three-dimensional structure, and the fact that $r_A$ of Cys-374 is 20–25 Å implies that the C-terminus lies on the side of the larger lobe, but the center of mass of this lobe can be located at either high or low radius. Nevertheless, answers to such questions should be easily provided once the spatial relationship between labeled chemical points is established, i.e., when the structure of monomeric actin becomes available or six intramolecular distances within actin are measured by FRET.

It should be noted that the radial coordinates here have been obtained from time-resolved rather than steady-state spectroscopy. The time-resolved technique made it possible to verify independently the proposed model of FRET in the filament by following the time course of the fluorescence decay (see Figure 3). While the model appears to be valid, an important question is how accurate the measured coordinates are.

We first consider parameters used for the Dale–Eisinger analysis (Table III). The values of the orientation factors, and the limits of the critical Förster distances shown there, are somewhat misleading as to the "realistic" limits of the uncertainty of the radial distances measured in this paper. The limits in Table III were computed for a transfer between a single donor and a single acceptor. In the filament, however, FRET may occur to four neighboring actin monomers. Each pair has a fixed, on the nanosecond time scale, D–A separation but a different angle between the transition moments of the donor and acceptor. Thus, in addition to the *dynamic* distribution of the D–A orientation caused by the mobility of the probes and the protein, this ensemble of probes creates a *static* distribution of acceptor orientations around each donor.

The effect of static averaging of the D and A orientation has been examined by Dale et al. (1979). For an *isotropic* distribution, the difference in transfer efficiency between statically and dynamically averaged cases has been demonstrated to be small as long as the transfer efficiency remains low (there is 15% difference at $E = 0.5$). Our case is, of course, different from that isotropic example. Nevertheless, we can expect that the presence of four acceptors will result in more averaging than for a single D–A pair and will narrow the range of possible $\kappa^2$ values, i.e., increase the accuracy of the measured distances.

Labels attached to Gln-41 possess a great deal of rotational freedom (Tables II and III). Under these conditions the major source of uncertainty in the FRET-based coordinates is the presence of a long link between the modified glutamine residue and the chromophoric portion of the dye. Our results would be difficult to interpret if, due to the flexibility of the link, FRET occurred between labels diversely oriented in space with different interprobe (and radial) distances. We think, however, that for the DNC–RHC pair such a situation does not exist since if it did, its effect on the nanosecond decay kinetics would be dramatic, similar to what was seen for the DNC–FLC pair in the presence of S1.

The effect of the physical size of the dye conjugated to Gln-41 on the apparent radial coordinate of this residue can be estimated with the help of Figure 1B. The measured radial distance of cadaverine-based labels is approximately 41 Å. This implies that the interprobe distance between actin 0 and the next monomer in the helix (0 to 1) is ~80–85 Å. The cadaverine portion of the labels and the labels themselves contribute about 20–25 Å to this (interprobe) distance (the two dyes have also a vertical separation). This brings the radial coordinate of Gln-41 to approximately 30 Å (see Figure 1B). This value has to be considered only as a lower limit for this coordinate since the precise orientation of the cadaverine portion of the label with respect to filament axis is unknown. Thus, one can rather confidently place Gln-41 between the middle and outer part of the filament ($r_A$ ~30–45 Å).

The radial coordinate of Cys-374 obtained here with two new probes turned out to be about 20–25 Å. This value is significantly smaller than the ~35 Å measured before (Taylor et al., 1981). There are two plausible reasons to explain this difference: (1) Both donor and acceptor used previously were rather bulky and much larger than either monobromobimane or 1,5-IAEDNS employed in this study. For eosin which was used by Taylor et al. (1981), the distance between the protein and the chromophoric portion of the dye is about 5–8 Å longer than in bimane. This fact leads to the conclusion that a large part of the discrepancy can be explained by the different size of the probes used. (2) Reactive derivatives of fluorescein, rhodamine, and eosin are difficult to purchase in very pure form, and as recently reported, samples of (iodoacetamido)-tetramethylrhodamine from two manufacturers have quite different absorption spectra (Takashi et al., 1986). Taylor et al. (1981) noted themselves that new batches of eosin gave considerably higher FRET efficiencies. Thus it is possible that poor purity of the labels can at least be partially responsible for the discrepancy.

The radial coordinate of the nucleotide bound to actin can be helpful in orienting the actin monomer in the filament if the exact position of the nucleotide base in the three-dimensional structure of the protein is known. Fortunately, recent photoaffinity labeling experiments identified Lys-336, Trp-356 (Hegyi et al., 1986), and Tyr-306 (Kuwayama & Yount, 1986) as amino acids in the actin sequence directly involved in the binding or located in close proximity of the nucleotide base. Residues 114–118 of actin were postulated to be involved in the binding of the phosphate moiety of the nucleotide (Barden & Kemp, 1987). Presumably, the position of the nucleotide will also be available from X-ray crystallography. In such a case we may be able to compare directly the FRET and the X-ray distances.

The binding of S1 to the filament had no effect on the radial coordinates of either Cys-374 or the nucleotide binding site. For the DNC–RHC, both attached to Gln-41, a small increase (~5 Å) of the radial coordinate was observed. These results do *not* mean, however, that S1 has no effect on the conformation of the actin molecule in the vicinity of either Cys-374 or the nucleotide binding site. In this paper we have demonstrated that S1 has a pronounced influence on the energy transfer between DNC and FLC attached to Gln-41 on different monomers. There is also evidence that S1 has some effect on Cys-374. All these data are consistent with the hypothesis that S1 binding results in local conformational changes of various parts of actin. If there is S1-induced

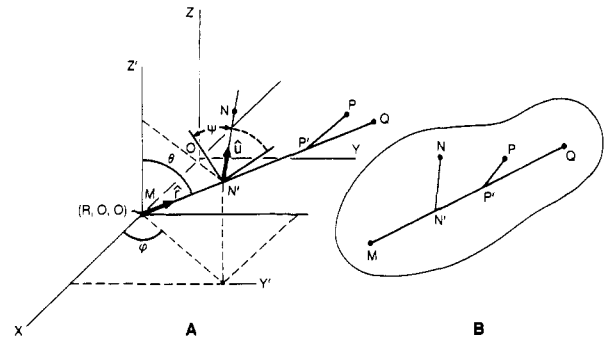


FIGURE 6: Four points, not all collinear, $M$, $N$, $P$, and $Q$, are in the rigid body shown at (B). A line (—) $MQ$ is drawn through two arbitrarily picked points. Perpendiculars from the other two points are dropped to $MQ$, meeting it at $N'$ and $P'$. This framework of points and lines is now placed in a coordinate system (A) so that $M$ is at $(R, 0, 0)$. The body continues to be associated with the framework and is therefore also positioned, but its ouline has been omitted for clarity.

"in-place" rotation of the monomer, it cannot be of great amplitude.

It has been recently reported that subfragment 1 assembles actin filaments into raft-like structures (Ando & Scales, 1985). One might wonder whether this phenomenon could complicate our interpretation of the FRET measurements in the presence of S1. There are three lines of evidence that argue against a possibility that "bundling" of actin by S1 could distort the data presented here. (1) The formation of bundles depends critically on the type and concentration of the anion present (Ando, 1987). The effect is almost completely extinguished at concentrations of $Cl^-$ of 20 mM and higher. In this work we have used chloride ion at 50 mM concentration. (2) The distance between two filaments in an assembled bundle is approximately 180 Å (Ando, 1987). Energy transfer over such a long distance is insignificant. (3) Since S1 has no apparent influence on the monomer orientation, in order to postulate any distortion of the data caused by bundling, one has to assume that the effects of a hypothetical S1-induced rotation and actin bundling on the fluorescence of the label(s) compensate each other, producing no measurable change in the emission properties of the donor(s). Such a coincidence seems unlikely.

We believe that the method of measuring the filament response to binding of proteins can be fully utilized with other macromolecular ligands of actin. Investigating the effect of S1 binding on the filament structure is probably only the beginning of using this approach to study the effect of heavy meromyosin on the filament and responses of F-actin when its regulatory system is present.

ACKNOWLEDGMENTS

We thank Professor L. Peller for helpful comments.

## APPENDIX

(A) Of the three translational and three rotational degrees of freedom of a rigid body, two translational degrees are considered immaterial (where, parallel to the filament, and where, around the filament, is the body); therefore, it may be anticipated that four relational parameters between body and axis must be obtained in order to position the body. Consider four not all collinear points, $M$, $N$, $P$, and $Q$, of the body and draw $\overline{MQ}$, and then draw perpendiculars to $\overline{MQ}$ from $N$ (to $N'$) and $P$ (to $P'$) (Figure 6B). Now place the body in a coordinate system so that $M$ comes to rest at $(R, 0, 0)$ (Figure 6A). $\overline{OM}$ is a radial distance to a point in the body, so measurement of $R$ supplies the missing translational coordinate. The conventional position vector of $N$ is $\hat{\imath} + \hat{r}\overline{MN'} + \hat{u}\overline{N'N}$, where [see Morales (1984) for a related treatment]

$$\hat{u} = [(\hat{r} \times \hat{k} \times \hat{r}) \cos \psi + (\hat{k} \times \hat{r}) \sin \psi]/\sin \theta \quad \text{(A1)}$$

The position vector is thus a function of the three orientational angles, $\theta$, $\phi$, and $\psi$. The $X$-, $Y$-, and $Z$-components of this vector are obtainable by taking its scalar product with $\hat{\imath}$, $\hat{\jmath}$, and $\hat{k}$, respectively. Alternatively, a point such as $N$ can be located by a vector whose $Z$-component is the same as the conventional, but whose $X$- and $Y$-components are $\rho_x$ and $\rho_y$, respectively. Since the two vectors position the same point, they must be equal, and their corresponding components must be equal. The $Z$-components are artifically equal, but this procedure separately relates $\rho_x$ and $\rho_y$ to orientational angles. Squaring and adding these two equations, we obtain an equation relating the square of the radial distance to point $N$, $\rho^2(N)$, to the orientational angles:

$$R^2 + \overline{MN'}^2 \sin^2 \theta + 2R\overline{MN'} \sin \theta \cos \phi - 2R\overline{N'N}[\cos \theta \cos \phi \cos \psi + \sin \phi \sin \psi] - 2\overline{MN'}\,\overline{N'N} \times \sin \theta \cos \theta \cos \psi + \overline{N'N}^2[1 - \sin^2 \theta \cos^2 \psi] = \rho^2(N) \quad \text{(A2)}$$

An entirely analogous equation is obtained for $\rho^2(P)$, except that corresponding intrabody distances for $P$ appear, and $\psi(N)$ is replaced by $\psi(N) + \Delta\psi$. The equation for $\rho^2(Q)$ is simpler in that it does not contain any $\psi$. The three experimentally measurable $\rho^2(N)$, $\rho^2(P)$, and $\rho^2(Q)$ are thus separately related to three orientational angles, $\theta$, $\phi$, and $\psi$. These three relations minimally determine the orientation of the body relative to the axis, and the fourth radial distance measurement, $R$, tells how far it is from the axis; thus a minimum of four radial distances must be measured in order to position a rigid body in relation to an axis. Of course, obtaining actual values of $\theta$, $\phi$, and $\psi$, i.e., actually solving the equations, requires knowledge of certain intrabody distances and of $\Delta\psi = \psi(P) - \psi(N)$. In principle, FRET can provide $MQ$, as well the three sides of the triangles $MNQ$ and $MPQ$, and from the solved triangles can be obtained $\overline{MN'}$, $\overline{N'N}$, $\overline{MP}$, and $\overline{P'P}$. Deduction of the intrabody angle, $\Delta\psi$, requires the additional FRET measurements of $\overline{NP}^2$ and application of the cosine law

$$\overline{NP}^2 - \overline{N'P'}^2 = \overline{N'N}^2 + \overline{P'P}^2 - 2\overline{N'N}\,\overline{P'P} \cos \Delta\psi \quad \text{(A3)}$$

The orientation of a body obtained by radial distance measurements is not absolute. This can be seen by analyzing the structure of eq A2. Let $\alpha$ be an angle in the first quadrant (I), and consider as its conjugate angles, $\pi - \alpha$ (II), $\pi + \alpha$ (III), and $2\pi - \alpha$ (IV). Then, if a solution set $(\theta, \phi, \psi)$ of eq A3 can be characterized as (I, I, I), the left-hand side of eq A2 is invariant to substituting (I, IV, IV), or (II, I, II), or (II, IV, III), so these other three are also solution sets. These four sets represent symmetrical orientations of the body that cannot be distinguished by radial distance measurements.

(B) We will show below that integration of normalized multicomponent decay curves in the presence and in the absence of acceptor leads to properly averaged efficiency of energy transfer.

Equation 4 can be rewritten:

$$\langle F(t)/F(0) \rangle = \sum_{u,v} p(u|v) \sum_{j=1}^{m} \alpha_j \exp(-t\theta_{uvj}) = \sum_{j=1}^{m} \sum_{u,v}^{n} \beta_{uvj} \exp(-t\theta_{uvj}) \quad \text{(B1)}$$

where $\beta_{uvj} = \alpha_j p(u|v)$ and $\theta_{uvj} = (1/\tau_{0j})(1 + S_{uv})$. The summations extend over all possible combinations of $u$, $v = 0$, 1, and 2.

Integration of eq B1 from $t = 0$ to $t = \infty$ yields

$$A = \int_0^\infty \langle F(t)/F(0)\rangle \, dt = \int_0^\infty \sum_{j=1}^{m}\sum_{u,v}\beta_{uvj}\exp(-t\theta_{uvj})\, dt$$
$$= \sum_{j=1}^{m}\sum_{u,v}\frac{\beta_{uvj}\exp(-t\theta_{uvj})}{-\theta_{uvj}}\Bigg|_0^\infty = \sum_{j=1}^{m}\sum_{u,v}\frac{\tau_{0j}\beta_{uvj}}{1+S_{uv}} \quad (B2)$$

In the absence of acceptors, $S_{uv} = 0$ and $p(0|0) = 1$; hence

$$A_0 = \sum_{j=1}^{m}\sum_{u,v}(\tau_{0j}\beta_{uvj}) = \sum_{j=1}^{m}(\tau_{0j}\alpha_j) \quad (B3)$$

and by substituting the expressions in eq B2 and B3 for $A$ and $A_0$, respectively, we obtain

$$\frac{A}{A_0} = \frac{\sum_{j=1}^{m}\sum_{u,v}\frac{\tau_{0j}\alpha_j p(u|v)}{1+S_{uv}}}{\sum_{j=1}^{m}\alpha_j\tau_{0j}} = \frac{\sum_{j=1}^{m}\alpha_j\tau_{0j}\sum_{u,v}\frac{p(u|v)}{1+S_{uv}}}{\sum_{j=1}^{m}\alpha_j\tau_{0j}} \quad (B4)$$

Assuming that there is no heterogeneity in $R_0$, the summations over $u$ and $v$ are identical for each lifetime component, and the terms containing $\alpha_j$ and $\tau_{0j}$ reduce, yielding

$$\frac{A}{A_0} = \sum_{u,v}\frac{p(u|v)}{1+S_{uv}} \quad (B5)$$

Bearing in mind that $\sum p(u|v) = 1$, we can now compute $1 - A/A_0$:

$$1 - \frac{A}{A_0} = \sum_{u,v}p(u|v)\frac{1+S_{uv}}{1+S_{uv}} - \sum_{u,v}p(u|v)\frac{1}{1+S_{uv}} = \sum_{u,v}p(u|v)\frac{S_{uv}}{1+S_{uv}} \quad (B6)$$

The last expression is identical to $\langle E\rangle$ in eq 3.

The ratio of the integrated areas under fluorescence decay curves in the presence and absence of acceptors is not affected by the lamp pulse. In that sense there is no error involved in calculating the ratio of $A/A_0$ from convoluted curves. However, if no deconvolution is performed, it is not obvious how to obtain $F(0)$. We have simulated the effect of the presence of acceptors for the data shown in Figure 4, using both a $\delta$-function and an experimental lamp profile and making a simplified assumption that $F(\max)$ can be used as a normalization factor instead of $F(0)$. The result was that, for samples possessing fluorescence characteristics similar to those in Figure 4, the error in $\langle E\rangle$ is about 4%.

## References


Amos, L. A. (1985) *Annu. Rev. Biophys. Bioeng. 14*, 291–313.

Ando, T. (1987) *J. Mol. Biol. 195*, 351–358.

Ando, T., & Scales, D. (1985) *J. Biol. Chem. 260*, 2321–2327.

Asakura, S. (1961) *Arch. Biochem. Biophys. 92*, 140–149.

Babcock, D. F. (1983) *J. Biol. Chem. 258*, 6380–6389.

Badea, M. G., & Brand, L. (1975) *Methods Enzymol. 61*, 378–425.

Badley, R. A., & Teale, F. W. J. (1969) *J. Mol. Biol. 44*, 71–88.

Barden, J. A., & Kemp, B. E. (1987) *Biochemistry 26*, 1471–1478.

Carlsson, L., Nyström, L.-E., Lindberg, U., Kannan, K. K., Cid-Dresdner, H., Lövgren, S., & Jörnvall, H. (1976) *J. Mol. Biol. 105*, 353–366.

Connellan, J. M., Chung, S. I., Whetzel, K., Bradley, L. M., & Folk, J. E. (1971) *J. Biol. Chem. 246*, 1093–1098.

Dale, R. E., Eisinger, J., & Blumberg, W. E. (1979) *Biophys. J. 26*, 161–194.

Egelman, E. H. (1985) *J. Muscle Res. Cell Motil. 6*, 129–151.

Egelman, E. H., & DeRosier, D. J. (1982) *Acta Crystallogr., Sect. A: Cryst. Phys., Diffr., Theor. Gen. Crystallogr. A38*, 796–799.

Egelman, E. H., & DeRosier, D. J. (1983) in *Actin: Structure and Function in Muscle and Nonmuscle Cells* (dos Remedios, C. G., & Barden, J., Eds.) pp 17–24, Academic: New York and London.

Egelman, E. H., Francis, N., & DeRosier, D. J. (1982) *Nature (London) 298*, 131–135.

Eisenthal, K. B., & Siegel, S. (1964) *J. Chem. Phys. 41*, 652–655.

Elzinga, M., & Phelan, J. (1984) *Proc. Natl. Acad. Sci. U.S.A. 81*, 6599–6602.

Fung, B. K.-K., & Stryer, L. (1978) *Biochemistry 17*, 5241–5248.

Grinvald, A., & Steinberg, I. Z. (1974) *Anal. Biochem. 59*, 583–598.

Grinvald, A., Haas, E., & Steinberg, I. Z. (1972) *Proc. Natl. Acad. Sci. U.S.A. 69*, 2273–2277.

Hanson, J. (1967) *Nature (London) 213*, 353–356.

Hegyi, G., Szilagyi, L., & Elzinga, M. (1986) *Biochemistry 25*, 5793–5798.

Hiratsuka, T., & Uchida, K. (1973) *Biochim. Biophys. Acta 320*, 635–647.

Houk, T. W., & Ue, K. (1974) *Anal. Biochem. 62*, 66–74.

Hudson, E. N., & Weber, G. (1973) *Biochemistry 12*, 4154–4161.

Huxley, H. E. (1972) in *The Structure and Function of Muscle* (Bourne, G. H., Ed.) pp 301–387, Academic, New York and London.

Kabsch, W., Mannherz, H. G., & Suck, D. (1985) *EMBO J. 4*, 2113–2118.

Katoh, T., Imae, S., & Morita, F. (1984) *J. Biochem. (Tokyo) 95*, 447–454.

Knight, P., & Offer, G. (1978) *Biochem. J. 175*, 1023–1032.

Kosower, E. M., & Pazhenchensky, B. (1980) *J. Am. Chem. Soc. 102*, 4983–4993.

Kosower, N. S., Kosower, E. M., Newton, G. L., & Ranney, H. M. (1979) *Proc. Natl. Acad. Sci. U.S.A. 76*, 3382–3386.

Kuwayama, H., & Yount, R. G. (1986) *Biophys. J. 49*, 454a.

Lorand, L., Rule, N. G., Ong, H. H., Furlanetto, R., Jacobsen, A., Downey, J., Oner, N., & Brunner-Lorand, J. (1968) *Biochemistry 7*, 1214–1223.

Lorand, L., Parameswaran, K. N., Velasco, P. T., Hsu, L. K.-H., & Siefring, G. E., Jr. (1983) *Anal. Biochem. 131*, 419–425.

Mihashi, K., & Wahl, P. (1975) *FEBS Lett. 52*, 8–12.

Miki, M., & Wahl, P. (1984) *Biochim. Biophys. Acta 786*, 188–196.

Miki, M., Barden, J. A., Hambly, B. D., & dos Remedios, C. G. (1986a) *Biochem. Int. 12*, 725–731.

Miki, M., Hambly, B. D., & dos Remedios, C. G. (1986b) *Biochim. Biophys. Acta 871*, 137–141.

Morales, M. F. (1984) *Proc. Natl. Acad. Sci. U.S.A. 81*, 145–149.

Mornet, D., & Ue, K. (1984) *Proc. Natl. Acad. Sci. U.S.A. 81*, 3680–3684.

Oosawa, F. (1983) in *Actin: Structure and Function in Muscle and Nonmuscle Cells* (dos Remedios, C. G., & Barden, J., Eds.) pp 69–80, Academic, New York and London.

Schutt, C., Strauss, N., & Lindberg, U. (1985) *J. Muscle Res. Cell Motil. 6*, 668.

Secrist, J. A., III, Barrio, J. R., Leonard, N. J., & Weber, G. (1972) *Biochemistry 11*, 3499–3506.

Spudich, J. A., & Watt, S. (1971) *J. Biol. Chem. 246*, 4866-4871.
Squire, J. (1981) in *The Structural Basis of Muscular Contraction*, pp 157-179, Plenum, New York and London.
Stokes, D. L., & DeRosier, D. J. (1987) *J. Cell Biol. 104*, 1005-1017.
Suck, D., Kabsch, W., & Mannherz, H. G. (1981) *Proc. Natl. Acad. Sci. U.S.A. 78*, 4319-4323.
Suck, D., Oefner, C., & Kabsch, W. (1984) *EMBO J. 3*, 2423-2430.
Tajima, Y., Kamiya, K., & Seto, T. (1983) *Biophys. J. 43*, 335-343.
Takashi, R. (1979) *Biochemistry 18*, 5164-5169.
Takashi, R. (1988) *Biochemistry 27*, 938-943.
Takashi, R., & Kasprzak, A. A. (1985) *Biophys. J. 47*, 26a.
Takashi, R., & Kasprzak, A. A. (1987) *Biochemistry 26*, 7471-7477.
Takashi, R., Ue, K., & Waldrip, C. (1986) *Biophys. J. 49*, 221a.
Tao, T., & Cho, J. (1979) *Biochemistry 18*, 2759-2765.
Tao, T., Lamkin, M., & Lehrer, S. S. (1983) *Biochemistry 22*, 3059-3064.
Taylor, D. L., Reidler, J., Spudich, J. A., & Stryer, L. (1981) *J. Cell Biol. 89*, 362-367.
Taylor, K. A., & Amos, L. A. (1983) in *Actin: Structure and Function in Muscle and Nonmuscle Cells* (dos Remedios, C. G., & Barden, J., Eds.) pp 25-26, Academic, New York and London.
Thomas, D. D., Seidel, J. C., & Gergely, J. (1979) *J. Mol. Biol. 132*, 257-273.
Torgerson, P. M., & Morales, M. F. (1984) *Proc. Natl. Acad. Sci. U.S.A. 81*, 3723-3727.
Weeds, A. G., & Taylor, R. S. (1975) *Nature (London) 257*, 54-56.
Yanagida, T., Nakase, M., Nishiyama, K., & Oosawa, F. (1984) *Nature (London) 307*, 58-60.
Yoshimura, H., Nishio, T., Mihashi, K., Kinosita, K., Jr., & Ikegami, A. (1984) *J. Mol. Biol. 179*, 453-467.

# Cross-Linking of Proteins by Aldotriose: Reaction of the Carbonyl Function of the Keto Amines Generated in Situ with Amino Groups†

A. Seetharama Acharya,* Youngnan J. Cho, and Belur N. Manjula
*Division of Hematology, Department of Medicine, Albert Einstein College of Medicine, 1300 Morris Park Avenue, Bronx, New York 10461, and The Rockefeller University, 1230 York Avenue, New York, New York 10021*
*Received September 1, 1987; Revised Manuscript Received January 13, 1988*

ABSTRACT: Nonreductive modification of proteins with glyceraldehyde forming 2-oxo-3-hydroxypropylated protein is mechanistically analogous to nonenzymic glycation reactions. The latent cross-linking potential of glyceraldehyde as a consequence of the reactivity of the carbonyl function of 2-oxo-3-hydroxypropyl groups of nonreductively modified protein has been now investigated. Reaction of RNase A (0.5 mM) with glyceraldehyde (20 mM) at pH 7.4 and 37 °C for 4 h resulted in the intermolecular cross-linking of the protein, with the concomitant development of a yellow chromophore with two new absorption bands having maxima around 305 and 375 nm. The product exhibited a fluorescence that had excitation and emission maxima around 365 and 450 nm, respectively. The presence of $NaCNBH_3$ during the reaction, which selectively reduces the Schiff base adducts of aldotriose to form 2,3-dihydroxypropyl groups on proteins, inhibited both the cross-linking reaction and the development of the absorption and fluorescence characteristics. The hydroxymethyl group of the aldotriose is not an essential moiety since the cross-linking potential of glyceraldehyde is comparable to that of glyceraldehyde 3-phosphate. The formation of cross-links appears to involve the carbonyl function of the keto amines resulting in the formation of Schiff base adducts (ketimine linkages) as the initial event. Consistent with this, incubation of 2-oxo-3-hydroxypropylated RNase A with [$^{14}$C]glycine ethyl ester resulted in the incorporation of the reagent into the protein. The cross-linking reaction was inhibited when the reaction of RNase A with glyceraldehyde was carried out in the presence of amino compounds, such as glycine ethyl ester, ethanolamine, glucosamine, and aminoguanidine. An equimolar amount of aminoguanidine inhibited the nonreductive incorporation of [$^{14}$C]glyceraldehyde into RNase A by nearly 85%. The inhibition of the cross-linking reaction by the aminoguanidine and other amino compounds is predominantly a consequence of the inhibition of the nonenzymic glycation of RNase A. The results of the present study demonstrate that the protein cross-linking by aldotriose under physiological conditions is latent and is a consequence of the reactivity of the carbonyl function of keto amines generated in situ with the amino groups of protein.

The reaction of glyceraldehyde (2,3-dihydroxypropionaldehyde), an aldotriose, with hemoglobin (Hb) is mechanistically similar to nonenzymic glycation reaction (Acharya & Manning, 1980). Just as in the case of nonenzymic addition of glucose to Hb (Holmquest & Schroeder, 1966; Wold, 1981; Brownlee & Cerami, 1981; Brownlee et al., 1984), the reversible Schiff base adducts of glyceraldehyde with the amino groups of Hb undergo Amadori rearrangement to form stable keto amine adducts (Figure 1). Consistent with this similarity in the mechanism of the reaction of aldohexose and aldotriose, many of the sites on HbA that are reactive toward glyceraldehyde in vitro are the same as those that are nonenzymically glycated (Acharya & Manning, 1980; Shapiro et al., 1981).

† This work has been supported by NIH Grants HL-27183 and AM-35869 to A.S.A. and HL-36025 to B.N.M. B.N.M. was an Established Investigator of the American Heart Association during the early phase of this work. A.S.A. is an Established Fellow of New York Heart Association.

0006-2960/88/0427-4522$01.50/0 